Chinese Journal of Oceanology and Limnology
Vol. 34 No. 1, P. 200-211, 2016
http://dx.doi.org/10.1007/s00343-015-4245-0

Wave-induced seepage and its possible contribution to the formation of pockmarks in the Huanghe (Yellow) River delta*

WANG Hu (王虎)[1], LIU Hongjun (刘红军)[1, 2, **], ZHANG Minsheng (张民生)[1, 2], WANG Xiuhai (王秀海)[1, 2]

[1] *Key Laboratory of Marine Environment and Ecology, Ministry of Education, Ocean University of China, Qingdao 266100, China*

[2] *College of Environmental Science and Engineering, Ocean University of China, Qingdao 266100, China*

Received Sep. 20, 2014; accepted in principle Jan. 5, 2015; accepted for publication Feb. 6, 2015

Abstract Wave-induced seepage and its possible contribution to the formation of pockmarks in the Huanghe (Yellow) River delta were investigated experimentally and numerically. Laboratory experiments were carried out to explore the response of a layered silty seabed with various saturation conditions under cyclic wave loads, in which the pore pressure and seepage-related phenomena were particularly monitored. Numerical models to simulate wave-induced seepage in the seabed were presented and evaluated, then applied to the Huanghe River delta. The experimental results show that the excess pore pressure decreases more rapidly at the surface layer, while the seepage-related phenomena are more pronounced when large cyclic loads are applied and the underlying layer is less saturated. The proposed numerical models were verified by comparing with the experiments. The calculated seepage depth agreed well with the depth of the pockmarks in the Huanghe River delta. The experimental and numerical results and the existing in-situ investigations indicate that the wave-induced seepage may be a direct cause of the pockmarks in the Huanghe River delta. Extreme storm waves and the dual-layered structure of hard surface layer and weak underlying layer are essential external and internal factors, respectively. Wave- or current-induced scour and transport are possible contributors to the reformation of pockmarks at a later stage.

Keyword: wave loads; seepage; excess pore pressure; pockmarks; Huanghe (Yellow) River delta

1 INTRODUCTION

Pockmarks are common geohazards on the seafloor, which usually appear with fluid flow and are described as crater-like depressions (King and MacLean, 1970; Hovland and Judd, 1988). Pockmarks are an interesting part of marine environmental dynamics that can threaten the stability of marine structures. Therefore, investigating their origin and evolution mechanism is of scientific and engineering significance. Pockmarks have been found worldwide using various detection techniques such as shallow seismic profiling, side-scan sonar, and multi-beam echo sounding (Prior et al., 1986; Andrews et al., 2010; Dandapath et al., 2010; Moss et al., 2012). Several genesis mechanisms were proposed in different regions, taking into account the differences in sediment sources and depositional environments; these include wave-induced shallow slides (Xu et al., 2009), active faulting (Dondurur et al., 2011), current-induced erosion (Kilhams et al., 2011), hydrate decomposition (Sultan et al., 2010), and gas release from deeper reservoirs (Salmi et al., 2011). While most of the studies focus on macroscopic surveys, very few have examined the micro-mechanism of pockmark evolution or conducted quantitative estimations.

The modern Huanghe (Yellow) River delta was

* Supported by the National Natural Science Foundation of China (No. 41072216) and the Science and Technology Development Program of Shandong Province (No. 2014GGX104007)
** Corresponding author: hongjun@ouc.edu.cn

formed by the rapidly-deposited sediments that have been carried by the Huanghe River since A.D. 1855, and has been continuously transformed by complex ocean dynamic factors. Pockmarks in the Huanghe River delta are described as circular or oval depressions ranging from a few meters to several hundred meters in diameter and no more than 2 m in depth, and may exist individually or in groups (Li et al., 2006; Xu et al., 2009). On-site investigations show no evidence of hydrate decomposition or natural gas leakage, and reveal very little fault activity since A.D. 1855. The slope of the seabed is less than 0.4°; therefore, landslides can be mainly ruled out. It is noteworthy that pockmarks are usually associated with fluid flow-related features such as seepage chimneys and mud volcanoes (Harrington, 1985; Judd and Hovland, 2007; Cathles et al., 2010; Dandapath et al., 2012), indicating that the seepage of pore fluid may be an important factor during pockmark formation. Waves are a major ocean dynamic load that may cause different types of seabed instabilities such as liquefaction, scour, and shear failure (Sumer and Fredsøe, 2002; Jeng, 2003). The Huanghe River delta experiences frequent storm surges (Ding et al., 1995). Pockmarks have developed at water depths of 8–12 m, where the seabed is affected by storm waves. Many investigations argue that wave loads severely affect geohazards such as pockmarks in the Huanghe River delta (Prior et al., 1986; Chang et al., 2000; Xu et al., 2009). Because the seabed in the Huanghe River is very flat we focus on the seepage caused by wave loads rather than ground water or other factors summarized by Santos et al. (2012).

Fluid flow-related features have been observed in the seabed under wave loads or other cyclic loads in laboratory and field tests (Clukey et al., 1985; Tzang and Ou, 2006; Chen et al., 2007). Laboratory tests on wave-induced seabed response include wave flume tests (Tzang and Ou, 2006; Xu et al., 2009), centrifugal model tests (Sassa and Sekiguchi, 1999), and one-dimension cylinder tests (Zen and Yamazaki, 1990; Chowdhury et al., 2006). The seabed in these tests was prepared to be homogeneous and saturated medium; however, the actual seabed is inhomogeneous and layered (Jia et al., 2007; Liu et al., 2013b) and the soil pores may contain a small amount of gas. For example, micro-bubbles were observed in laboratory wave flume tests (Tzang and Ou, 2006) and field measurements (Mory et al., 2007). The seabed stability will be significantly affected by the saturation of seabed soil (Yamamoto et al., 1978; Sakai et al., 1992; De Groot et al., 2006). Numerous models were developed to simulate the seabed response under wave loads (Yamamoto et al., 1978; Jeng, 2003) based on the consolidation theory proposed by Biot (1941), and a series of models were established to explore the storm wave-induced seabed response in the Huanghe River delta (Yang et al., 1995; Liu et al., 2006, 2013a). In this paper, the wave-induced pore pressure response of a silty seabed is investigated through laboratory experiments and numerical models, focusing on the effects of the layered structure and seabed saturation on the seepage processes. The relation between wave-induced pore pressure and seepage-related phenomena are discussed and the possible contribution of wave-induced seepage to the formation of pockmarks in the Huanghe River delta is discussed.

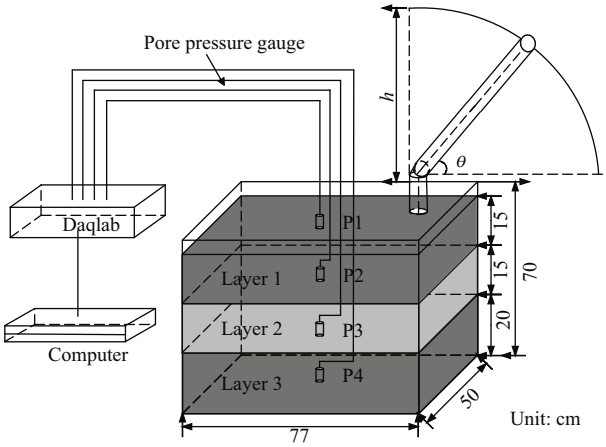

Fig.1 Sketch of experimental set-ups

h: water depth; *θ*: rotation angle; P1–P4: pressure transducers.

2. MATERIAL AND METHOD

2.1 Laboratory experiments

The testing apparatus consisted of an airtight tank (77 cm L×50 cm W×70 cm H), a cyclic loading system and a pore pressure acquisition system (Fig.1). The bottom and three sides of the tank were made of stainless steel, while the front and the top surfaces were made of toughened glass for observations and measurements. A pipe was connected to the top of the tank; this pipe could be rotated in the vertical plane with a rotation angle θ from 0° to 90°; thus, the water head could be changed to generate cyclic vertical pressure to simulate wave loads. An array of piezoresistive pore pressure transducers (Φ20 mm× 53 mm, full range 5 psi, accuracy 0.2%; Nanjing Hydraulic Research Institute, China) were connected

Table 1 Test parameters

Test	Cyclic loads		Layer 1		Layer 2		Layer 3	
	P_0 (kPa)	T (s)	S_r (%)	ρ (g/cm^3)	S_r (%)	ρ (g/cm^3)	S_r (%)	ρ (g/cm^3)
1	8	8–10	97.4	1.85	96.6	1.84	94.0	1.83
2	10	8–10	96.8	1.83	99.1	1.85	94.0	1.80
3	12	6–8	95.3	1.86	94.5	1.85	96.3	1.88
4	8	6–8	96.1	1.85	91.4	1.81	96.3	1.86
5	10	6–7	98.7	1.89	91.6	1.83	93.3	1.83
6	12	6–7	94.3	1.80	92.0	1.78	96.7	1.81
7	8	5–6	96.8	1.84	84.4	1.75	88.1	1.77
8	10	5–6	96.7	1.84	83.0	1.73	95.9	1.83
9	12	5–6	95.2	1.84	80.4	1.70	93.1	1.82

P_0: dynamic pressure amplitude at seabed surface; T: wave period; S_r: saturation; ρ: soil density.

to a DAQLab2005 acquisition system (Iotech, Cleveland, USA) to measure the pore pressure.

The soil, composed mainly of feldspar and quartz, was collected from the tidal flat of the Huanghe River delta. It is a typical silt with specific gravity ρ_s=2.71, plasticity index I_P=9.4, median particle size d_{50}=0.041 mm, and clay content m=12.2%. The soil samples were dried, crushed, mixed with water and stirred well to mud consistency. A chemical reagent, Na_2O_2 powder, was added to the mud where it reacted with the water ($2Na_2O_2+2H_2O=4NaOH+O_2\uparrow$) and produced oxygen gas. The small gas bubbles were enclosed in the soil pores so that the soil saturation could be lowered. The seabed model had three layers (Fig.1) from top to bottom: Layer 1 (15 cm), Layer 2 (15 cm), and Layer 3 (20 cm). Layer 1 and Layer 3 were saturated or nearly saturated while the saturation of Layer 2 ranged from high to low, simulating a hard surface layer and an unsaturated weak underlying layer. The transducers (P1–P4) were saturated and calibrated in static water, and then deployed at different depths (d=0 cm, d=-15 cm, d=-30 cm, and d=-45 cm) before the mud was placed into the tank and the lid sealed. The pipe was carefully filled with water to a predetermined height h, and then was tipped to a certain angle so that the water level was halfway between the maximum and minimum levels. The seabed was left for ten days or longer until a self-weight consolidation was achieved; the normal consolidation of the seabed was considered to be complete when the measured pore pressure was equal to the hydrostatic pore pressure.

The pipe was rotated repeatedly in the vertical plane, creating cyclic water loads on the model seabed surface. The fluctuation of the water pressure resembled a sine wave with periods ranging from 5 to 10 s. The amplitude of the pressure was set as 8, 10, and 12 kPa. The pore pressure was measured throughout the tests at a sampling frequency of 3 Hz. The experimental phenomena was recorded by a camera in real time. The cyclic loading was stopped when new phenomena and pore pressure changes were no longer observed. For each layer before and after testing, the soil density was measured by weighing a container with constant volume (100 mL), the water content was measured by the oven drying method, and the saturation could then be determined. After each test the tank was cleaned up and the above procedures were repeated in the next test. The design parameters of all the tests are listed in Table 1.

2.2 Numerical models

We used the finite element software Swandyne II (Chan, 1995) with the *u-p* formulation of Biot's equation, which has been proved to be effective in wave-induced pore pressure simulations (Dunn et al., 2006; Liu et al., 2013a). The governing equations under a two-dimensional plane strain are expressed as follows:

$$\frac{\partial \sigma'_x}{\partial x}+\frac{\partial p}{\partial x}+\frac{\partial \tau_{xz}}{\partial z}-\rho\frac{\partial^2 u_x}{\partial t^2}=0, \tag{1}$$

$$\frac{\partial \tau_{xz}}{\partial x}+\frac{\partial \sigma'_z}{\partial z}+\rho g+\frac{\partial p}{\partial z}-\rho\frac{\partial^2 u_z}{\partial t^2}=0, \tag{2}$$

$$\frac{1}{Q}\frac{\partial p}{\partial t}+\frac{\partial \varepsilon}{\partial t}-k\nabla^2 p-k\rho_f\frac{\partial^2 \varepsilon}{\partial t^2}=0, \tag{3}$$

where u_x and u_z are the displacements of the soil skeleton, σ'_x and σ'_z are the effective stresses, τ_{xz} is the shear stress, p is the pore pressure, ρ_f is the pore fluid

Table 2 Wave parameters

Return period of wave	Wave length L (m)	Wave height H (m)	Wave period T (s)	Water depth h (m)	Dynamic pressure P_0 (kPa)
1 year	40	2.0	5.0	10	3.91
50 years	88	6.7	8.6	10	25.92

Table 3 Soil parameters

Layer	Soil density ρ (g/cm^3)	Specific weight G_s	Void ratio e	Saturation S_r	Elastic modulus E (MPa)	Poisson's ratio μ
1	1.99	2.7	0.69	0.961	1	0.33
2	1.86	2.72	0.9	0.904	0.1	0.33
3	1.89	2.71	0.9	0.967	1	0.33

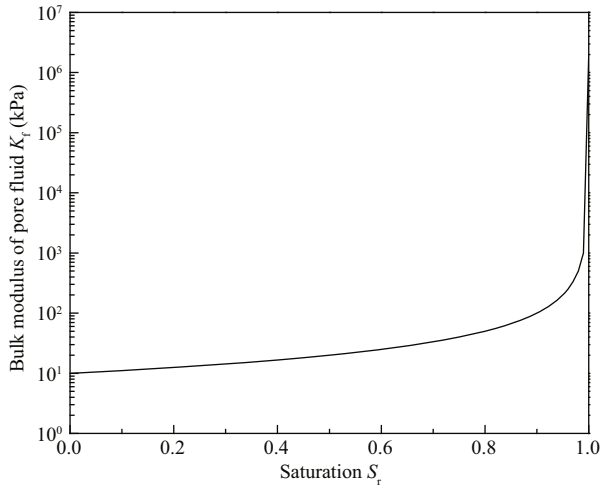

Fig.2 Relationship between soil saturation and bulk modulus of pore fluid

density, ε is the volumetric strain of the soil, ρ is the soil density, Q is the bulk modulus of the soil, and k is the soil permeability. ε, ρ, and Q are expressed as follows:

$$\rho = n\rho_f + (1-n)\rho_s, \tag{4}$$

$$\varepsilon = \frac{\partial u_x}{\partial x} + \frac{\partial u_z}{\partial z}, \tag{5}$$

$$\frac{1}{Q} = \frac{1-n}{K_s} + \frac{n}{K_f}, \tag{6}$$

where n is the soil porosity, ρ_s is the specific gravity, and K_s and K_f are the bulk modulus of the soil skeleton and pore fluid, respectively. The gas content in the soil pores is described by the saturation S_r, and the relationship between K_f and S_r is expressed as follows:

$$\frac{1}{K_f} = \frac{1}{K} + \frac{1-S_r}{P_0}, \tag{7}$$

where K is the bulk modulus of pure water. The relationship between K_f and S_r in the case of P_0=10 kPa and K=2 MPa is shown in Fig.2. Clearly, the magnitude of K_f changes dramatically as S_r increases. Thus, the effects of gas content on pore pressure can be explained by Eq.7.

First, we developed the numerical models to evaluate the laboratory experiment results. The seabed surface was set as a drainage boundary and the bottom and the two sides were impermeable rigid boundaries. We used 8–4-noded elements (8 solid nodes and 4 fluid nodes) in the numerical model. A linear-elastic relationship of the soil was selected to simulate the wave-induced transient pore pressure. The soil density and saturation parameters are taken from Table 1. Other parameters are: permeability k=2.5×10^{-6} cm/s, elastic modulus E=1 MPa, and Poisson's ratio μ=0.3 based on previous experience and trial computation results.

Then, numerical models were developed to explore the wave-induced seepage in the Huanghe River delta. Pockmarks and other geohazards in the Huanghe River delta appear mostly at water depths of 8–12 m and with a slope gradient of less than 0.4° (Prior et al., 1986; Li et al., 2006). Therefore, we chose a water depth of 10 m and assumed a horizontal seabed. Two types of wave with different return period were applied, based on previous studies (Yang et al., 1995; Liu et al., 2006, 2013a), as shown in Table 2. The dynamic pressure P_s on the seabed surface can be computed from the linear wave theory:

$$P_s = P_0 \sin(\eta x - \omega t),$$
$$P_0 = \frac{\rho_f g H}{2\cosh(\eta h)}, \tag{8}$$

where H is the wave height; η is the wave number, with η=2π/L, L is the wave length; h is the water depth; ω is the angular frequency, with ω=2π/T, where T is the wave period and t is time. The seabed in the Huanghe River delta is made up of silty soils with high compressibility, high water content and low permeability; moreover, a thin hard layer appears at

the seabed surface in some areas (Feng et al., 1999; Jia et al., 2007), which may have significant effects on the pore pressure response (Liu et al., 2013a). Therefore, two seabed models were considered: a homogeneous one and a three-layer one with a hard surface layer and an unsaturated weak underlying layer, corresponding to the models in the laboratory experiments. The simulated seabed was set with a width of one wavelength, a depth of half a wavelength, and horizontal grid spacing of 1 m. Layer 1 as the top layer of the three-layer seabed had a depth of 2 m and grid spacing of 0.25 m. The underlying layer, Layer 2, had a depth of 10 m and grid spacing of 0.5 m. The bottom layer, Layer 3, had a grid spacing of 1 m. The homogeneous seabed had the properties of Layer 1 throughout the model and the vertical grid spacing was the same as the three-layer seabed. The boundary conditions were the same as those in the laboratory experimental models. The soil parameters are listed in Table 3.

3 RESULT

3.1 Pore pressure response in the laboratory experiments

Two different experimental conditions—Test 1 and Test 9 are discussed here as examples. The seabed was nearly homogeneous (Table 1) and the amplitude of the wave load was the smallest (8 kPa) in Test 1. The saturation of Layer 2 was the lowest (80%) and the amplitude of the wave load was the largest (12 kPa) in Test 9. The excess pore pressure is defined as the difference between the measured value and the hydrostatic pore pressure. As shown in Fig.3, the results of Test 1 and Test 9 only show transient pore pressure (TPP) but no residual pore pressure (RPP). No obvious phase lag is seen from the enlarged TPP records (Fig.3, right panels). Generally, the TPP decreases at first and then increases with depth. The TPP decreases from 8 kPa at the seabed surface to 6.8 kPa at depth d=-15 cm, and remains nearly unchanged downward to depth d=-30 cm, then increases slightly at depth d=-45 cm (Fig.3a). The TPP decreases much faster with depth in Test 9 (Fig.3b) than in Test 1 (Fig.3a); the TPP is 12 kPa at the seabed surface and decreases rapidly to 4 kPa at d=-15 cm, and then it rebounds to 6 kPa at d=-30 cm and does not decrease any further at depth d=-45 cm. In summary, only TPP but no RPP was found in the seabed under cyclic loads, and only amplitude reduction but no phase lag of TPP was observed with depth.

The amplitude of the dynamic pressure at the seabed surface is denoted as P_0 and the amplitude of TPP in the seabed is denoted as P. The variations of P/P_0 with depth in all the nine tests are shown in Fig.4. Pore pressure damping occurs mainly near the seabed surface within Layer 1 and tends to be moderate below d=-15 cm. The three columns of Fig.4 show (from left to right) that pore pressure damping is accelerated because of the decreased saturation of Layer 2. Comparing the rows in Fig.4 (from top to bottom) indicates that pore pressure damping is enhanced as the external load is increased. In summary, pore pressure damping is affected by three factors: the layered structure of the seabed, the saturation of the seabed soil, and the external load. The damping occurs mainly in the surface layer, and it is intensified by larger external loading and lower saturation of the underlying layer.

3.2 Experimental phenomena

Seepage-related phenomena were observed on different scales in the tests. Seepage channels were formed in the seabed and pore fluid (mainly pore water, mixed with a small amount of gas micro-bubbles in some tests) flowed out of the seabed through these channels. Fine sediments were transported by the pore fluid, and mud volcanoes were formed on the seabed surface (Fig.5). The seepage channels were a few millimeters wide and less than 5 cm in depth near the seabed surface in Test 1 because of the small external load (8 kPa) and high saturation (96%) of the homogeneous seabed. The seepage channels expanded to 2 cm in width and 30 cm in depth in Test 9 with the increased external load and the decreased saturation of Layer 2. In addition, small gas bubbles were observed in some tests that featured a lower saturation of Layer 2. With Test 9 for example, as the cyclic loading continued, the gas that was initially scattered in the soil pores gradually converged to form micro-bubbles (Fig.5a, 0.1 cm in diameter) that developed into large bubbles (Fig.5c, 1–2 cm in diameter). Finally, the gas bubbles flowed to the seabed surface along with the pore water (Fig.5b, d, e). Moreover, the transport of bubbles was faster and the seepage channels became wider and deeper during the above process (Fig.5b, c, d, e). The micro-volcanoes on the seabed surface are shown in Fig.5f. In general, the larger-scale seepage-related phenomena appeared when larger cyclic loading was applied and the underlying layer was less saturated.

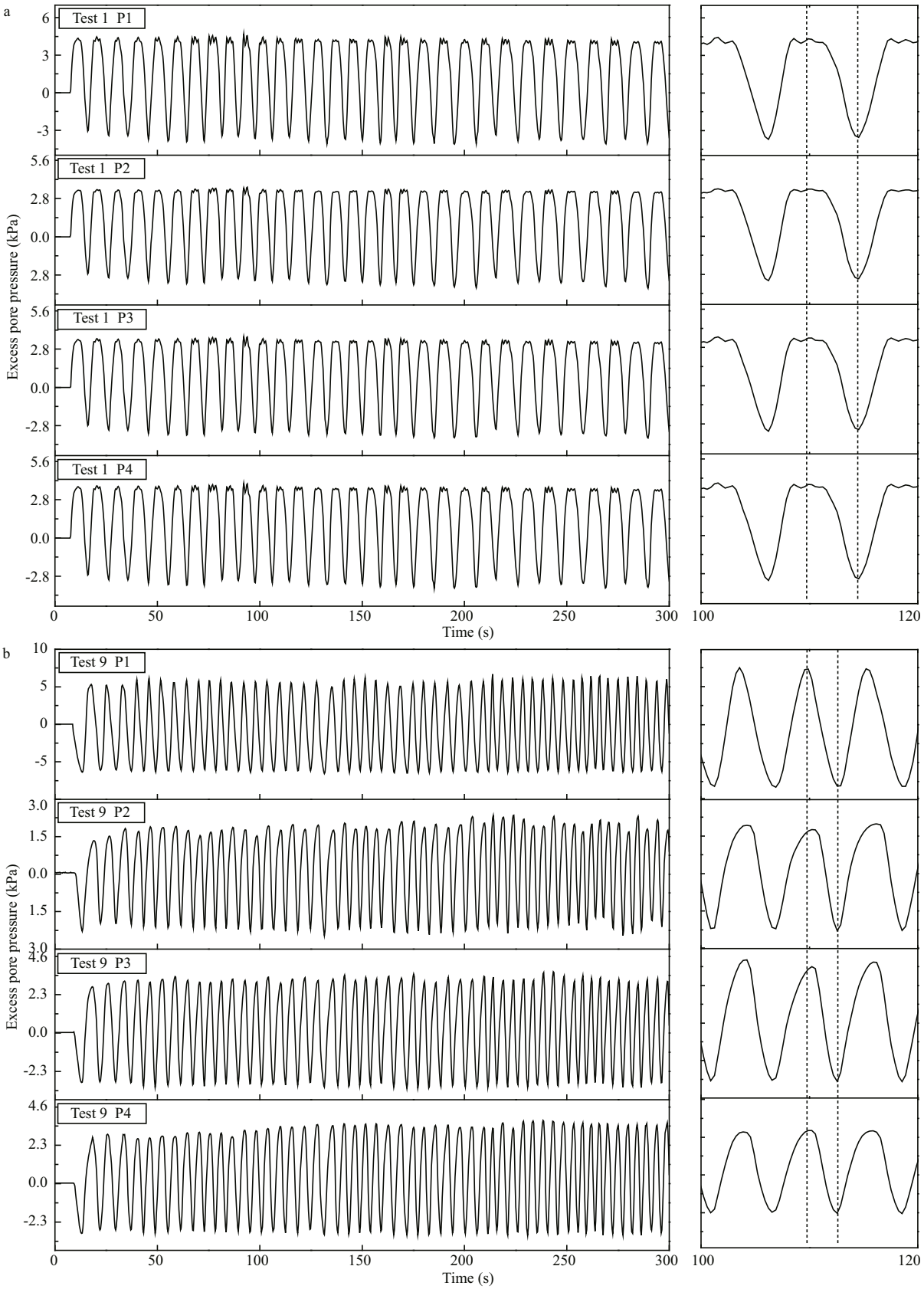

Fig.3 Pore pressure response

a. Test 1; b. Test 9.

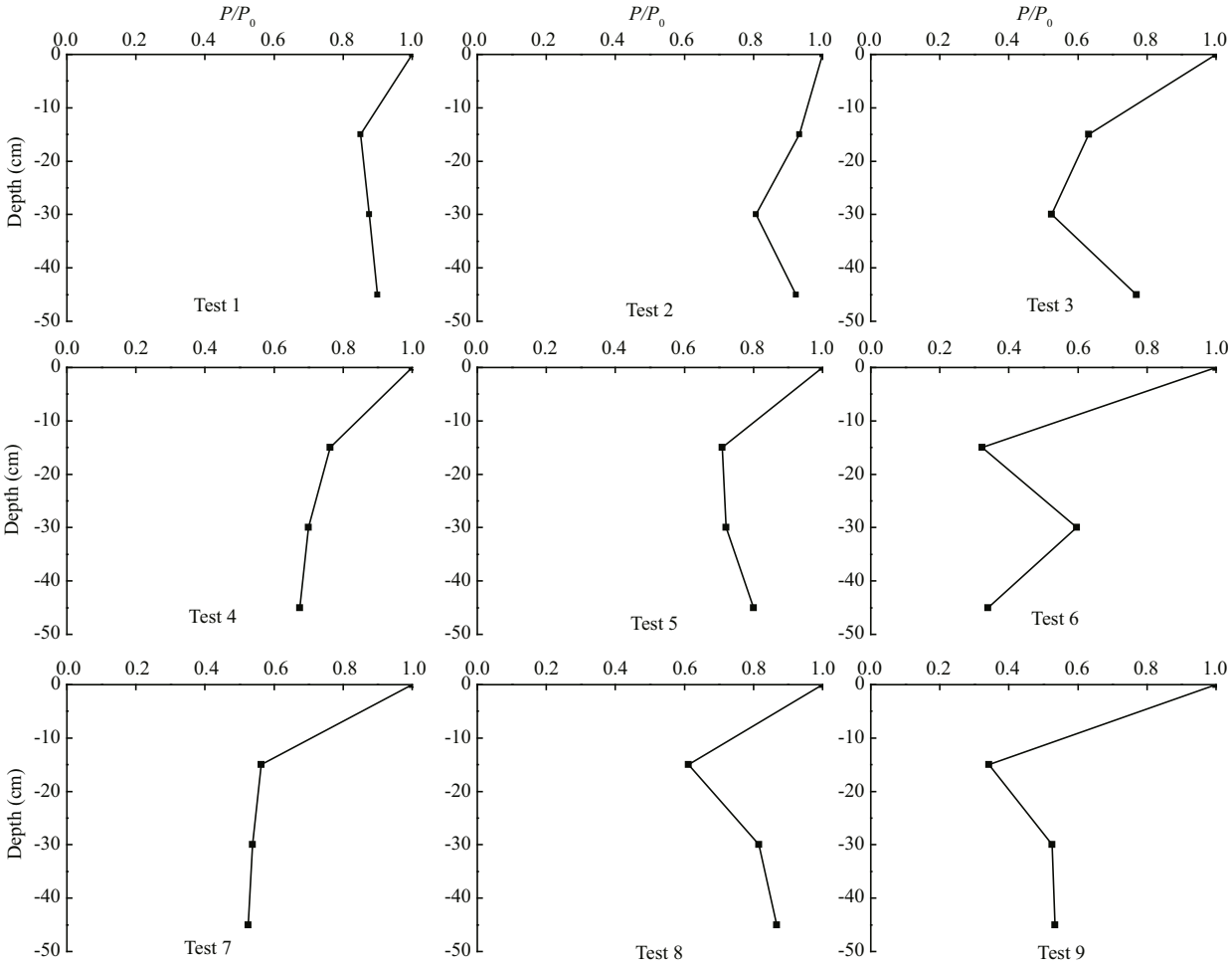

Fig.4 Pore pressure damping with seabed depth

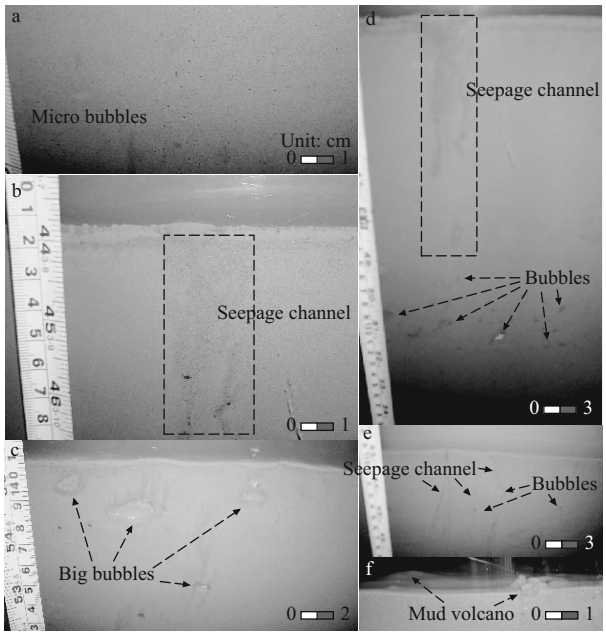

Fig.5 Seepage-related phenomena

a. micro bubbles; b. micro bubbles in seepage channels; c. expanded bubbles near seabed surface; d. extended seepage channels; e. sediment transported by seepage; and f. mud volcanoes.

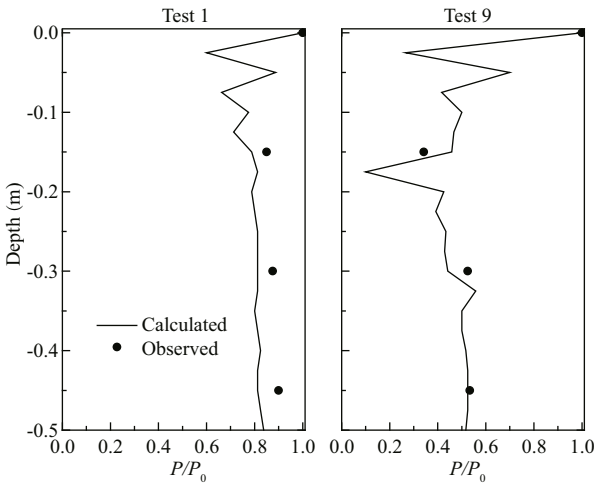

Fig.6 Comparison between experimental and numerical results

3.3 Numerical results

A vertical profile at the center of the seabed model was selected to output the pore pressure data. The results of Test 1 and Test 9 (Fig.6) show a good

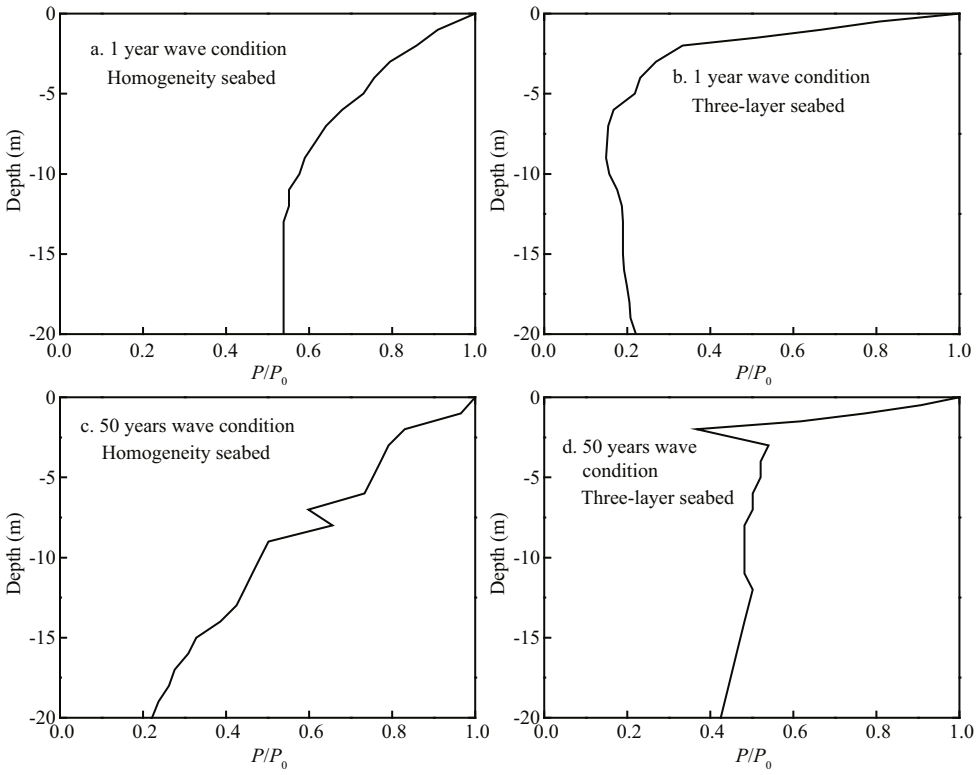

Fig.7 Wave-induced pore pressure in the Huanghe River delta

agreement between the numerical results and the experimental ones, indicating that the proposed model can simulate the seabed's pore pressure response under cyclic loads.

The variation of P/P_0 along depth with different return period (one year and 50 years) of waves and different seabed models (homogeneous and 3-layer seabed) are shown in Fig.7. When the seabed is homogeneous, the TPP decreases more rapidly in the surface layer under the wave with 50-years return period than under the wave with one-year return period, demonstrating the effect of the wave load. For the same wave loads, the TPP decreases faster in the surface layer of the three-layer seabed than in the homogeneous seabed, demonstrating the effect of the layers and the saturation of the seabed.

4 DISCUSSION

4.1 Relationship between pockmarks and wave-induced seepage

Seepage-related phenomena were caused by external cyclic loads, and were more prominent when the external loads increased. Assuming that the loads represent waves over the seabed, our data suggests that in the real ocean environment the seepage is caused by wave action, and the size of the seepage channels and mud volcanoes is enlarged by storm waves. The erupted fine sediments may be suspended and transported by currents (Hammer et al., 2009; Pau et al., 2014), and erosion is more likely to occur near the seepage channels where the soils are weakened. Thus, pockmark-like landforms may be formed. The above description can be verified by the remnant seepage channels and mud volcanoes along with pockmarks reported in previous studies (Harrington, 1985; Judd and Hovland, 2007; Cathles et al., 2010).

The seepage-related phenomena observed in our tests were enhanced by the gas content in the seabed soil; these processes were acknowledged in previous work (De Groot et al., 2006; Santos et al., 2012). Because the seabed is covered with seawater, it is usually modeled as consisting of soil skeleton and pore water. However, seabed soil actually contains soil skeleton, water, and gas. Pore water and pore gas are collectively called pore fluid. Although no hydrate decomposition or natural gas leakage was found in the Huanghe River delta, gas may be caught in a rapidly deposited seabed. Gas may also be generated by the decomposition of organic material in the seabed. Generally, a small amount of gas is enclosed in the soil pores in the seabed of the Huanghe River

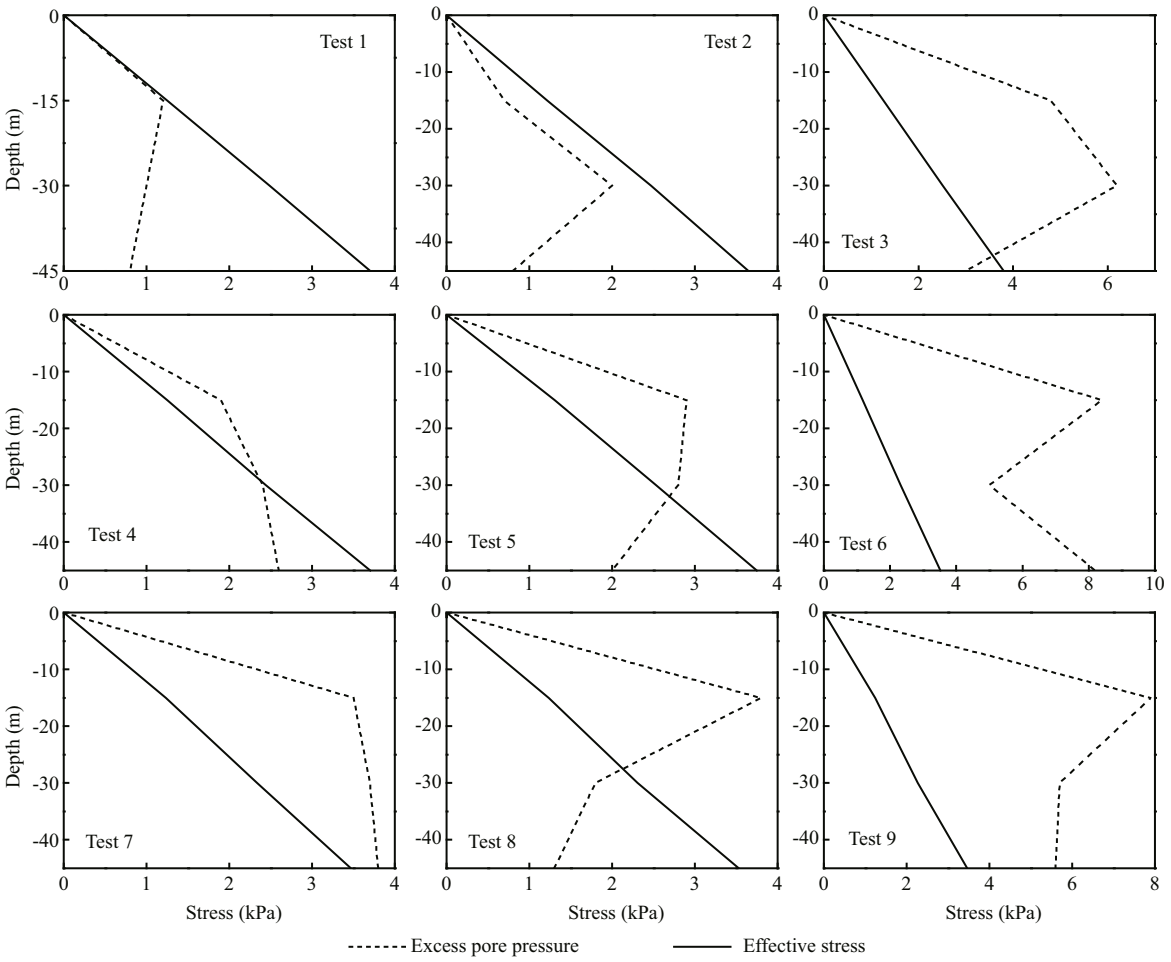

Fig.8 Seepage estimation in the experiments

delta (Jia et al., 2007; Xu et al., 2010). Extreme storm waves will cause the enclosed gas to shift and converge and drain out of the seabed, promoting upward seepage and contributing to the formation of pockmarks.

On a microscopic scale, when excess pore pressure is generated by cyclic wave loads, an upward hydraulic gradient is generated in the seabed. The seabed is usually taken as isotropic to simplify calculations; however, it is actually anisotropic and even seabed models created in the laboratory are not completely isotropic. Seepage tends to occur along the weakness zones in the seabed. Thus, individual seepage channels rather than complete liquefaction of the seabed are observed in laboratory tests and field investigations (Jia et al., 2007; Liu et al., 2012). The criterion for wave-induced seepage can be expressed as:

$$\sigma'_{v0} \le \Delta P = P_0 - P\,, \tag{9}$$

where σ'_{v0} is the initial vertical effective stress and can be computed by $\sigma'_{v0} = \sum \rho_i g d_i$; ρ_i is the soil density, d_i is the layer thickness, and ΔP is the excess pore pressure (Zen and Yamazaki, 1990). According to Eq.9, seepage will be more prominent if the TPP decreases more rapidly with depth, which can explain the findings in Section 3.2.

The variation of σ'_{v0} and ΔP with depth in all nine tests are shown in Fig.8. We can estimate whether or not seepage would happen by comparing the two lines. Seepage did not occur in Test 1 or Test 2. The maximum seepage depth is about 15 cm in Test 4 and Test 8, 30 cm in Test 3 and Test 5, and more than 45 cm in Tests 6, 7, and 9. The trend of the maximum seepage depth (Fig.8) is in agreement with the observation in Fig.5, but the calculated values are slightly larger than the observed values, probably because the naked eye cannot see some small seepage channels inside the seabed. The above analysis indicates that seepage is a macro-phenomenon caused by wave-induced excess pore pressure at the microscopic level. We can estimate the wave-induced seepage via Eq.9.

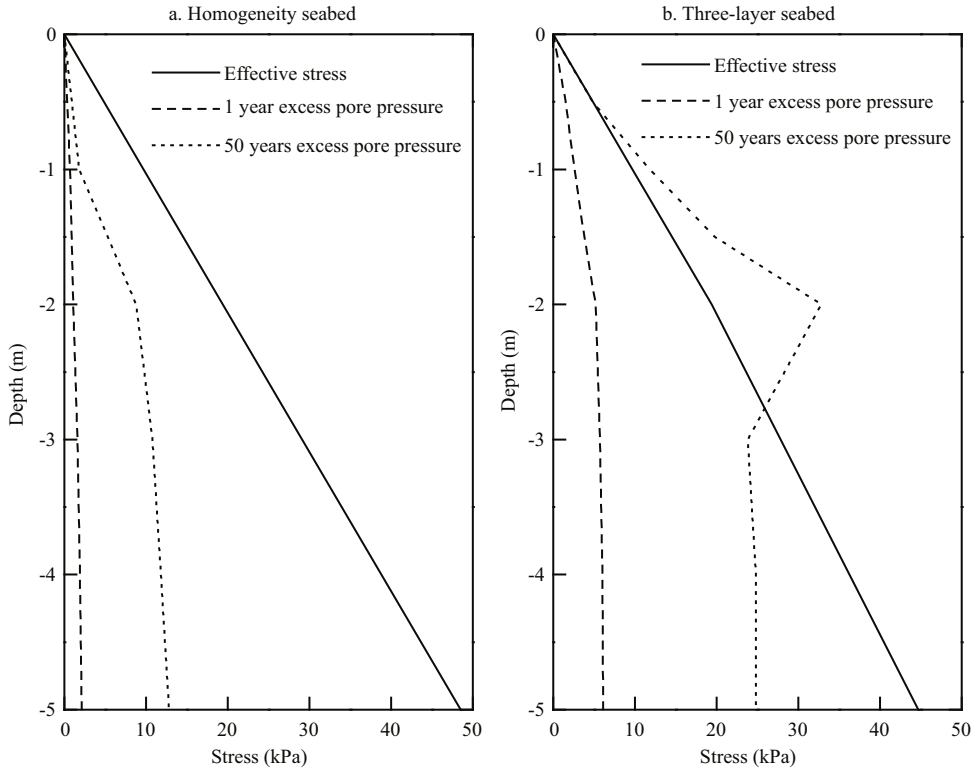

Fig.9 Wave-induced stress and seepage in the Huanghe River delta

4.2 Genesis mechanism of pockmarks in the Huanghe River delta

The variations of ΔP and σ'_{v0} are shown in Fig.9. Seepage does not occur in the homogeneous seabed for that ΔP is generally smaller than σ'_{v0} under both the two types of waves (Fig.9a). In the three-layer seabed, ΔP is smaller than σ'_{v0} under the wave with return period of one year, but larger than σ'_{v0} at depths of 2–3 m under the wave with return period of 50 years, indicating that the biggest seepage depth ranges from 2 to 3 m under the seabed surface (Fig.9b). As the calculated seepage depth is slightly bigger than the actual value, the calculated seepage depths are in good agreement with the measured depth of the pockmarks (within 2 m) in the subaqueous Huanghe River delta (Li et al., 2006; Xu et al., 2009). Figure 9 also shows that larger wave loads lead to larger ΔP, indicating that extreme wave conditions such as storm waves can dramatically increase seabed seepage. Meanwhile, larger ΔP exists in the three-layer seabed, indicating that the combination of a hard surface layer and an unsaturated underlying layer can significantly enhance the wave-induced seepage.

Based on the experimental and numerical results of this study we deduce the following points regarding the formation mechanism of pockmarks in the subaqueous Huanghe River delta. The distribution of the hard surface layer and unsaturated weak underlying layer of the seabed is a critical internal factor. Extreme storm waves are essential external factors. The wave-induced excess pore pressure and seabed seepage are the micro-mechanisms in the pockmark formation process. Seepage-related features such as seepage channels and mud volcanoes are the early forms of pockmarks. Erosion and transport caused by waves or currents may contribute to reformation of pockmarks at a later stage.

5 CONCLUSION

Wave-induced seepage and its possible contribution to the formation of pockmarks in the Huanghe River delta were explored experimentally and numerically. Conclusions can be drawn as follows:

Laboratory experiments indicate that transient pore pressure but no residual pore pressure occurred in the silty seabed under cyclic loads, and only amplitude damping but no phase lag of the transient pore pressure was observed with increasing depth of the seabed. With increasing amplitudes of the cyclic loads and lower saturation of the underlying layer, the transient pore pressure decreased more rapidly in the surface layer and the size of the seepage-related

features such as seepage channels and mud volcanoes increased.

Pockmarks are directly caused by seabed seepage, and the wave-induced excess pore pressure is critical in the estimation of seabed seepage. The model based on Biot's consolidation theory can simulate the wave-induced pore pressure well when considering the layers and saturation of the seabed. Extreme wave conditions combined with a hard surface layer and an unsaturated weak underlying layer can significantly enhance the seabed seepage.

Our study indicates the following points regarding the formation mechanism of pockmarks in the Huanghe River delta. The hard surface layer and unsaturated weak underlying layer in the seabed is a critical internal factor, while extreme wave conditions such as storm waves are an essential external factor. Seepage-related features such as seepage channels and mud volcanoes are the early forms of pockmarks. Erosion and transport caused by waves or currents may contribute to reformation of pockmarks at a later stage.

References

Andrews B D, Brothers L L, Barnhardt W A. 2010. Automated feature extraction and spatial organization of seafloor pockmarks, Belfast Bay, Maine, USA. *Geomorphology*, **124**(1-2): 55-64.

Biot M A. 1941. General theory of three-dimensional consolidation. *Journal of Applied Physics*, **12**(2): 155-164.

Cathles L M, Su Z, Chen D F. 2010. The physics of gas chimney and pockmark formation, with implications for assessment of seafloor hazards and gas sequestration. *Marine and Petroleum Geology*, **27**(1): 82-91.

Chan A H C. 1995. User Manual for Diana-Swandyne II-Dynamic Interaction and Nonlinear Analysis Swansea Dynamic Program Version II. England: Department of Civil Engineering, University of Glasgow.

Chang R F, Chen Z R, Chen W M et al. 2000. The recent evolution and controlling factors of unstable seabed topography of the old Yellow River subaqueus delta. *Journal of Ocean University of Qingdao*, **30**(1): 159-164. (in Chinese with English abstract)

Chen Y Y, Liu H J, Jia Y G et al. 2007. Qualitative study on mechanism of liquefaction and seepage of seabed structure silty soil under cyclic loads. *Rock and Soil Mechanics*, **28**(8): 1 631-1 635. (in Chinese with English abstract)

Chowdhury B, Dasari G R, Nogami T. 2006. Laboratory study of liquefaction due to wave-seabed interaction. *Journal of Geotechnical and Geoenvironmental Engineering*, **132**(7): 842-851.

Clukey E C, Kulhawy F H, Liu P L F. 1985. Response of soils to wave loads: experimental study. *In*: Chaney R C, Demars K R eds. Strength Testing of Marine Sediments: Laboratory and In-Situ Measurements, ASTM STP 883. American Society for Testing and Materials, Philadelphia. p.381-396.

Dandapath S, Chakraborty B, Karisiddaiah S M et al. 2010. Morphology of pockmarks along the western continental margin of India: employing multibeam bathymetry and backscatter data. *Marine and Petroleum Geology*, **27**(10): 2 107-2 117.

Dandapath S, Chakraborty B, Maslov N et al. 2012. Characterization of seafloor pockmark seepage of hydrocarbons employing fractal: a case study from the western continental margin of India. *Marine and Petroleum Geology*, **29**(1): 115-128.

De Groot M B, Bolton M D, Foray P et al. 2006. Physics of liquefaction phenomena around marine structures. *Journal of Waterway*, *Port*, *Coastal*, *and Ocean Engineering*, **132**(4): 227-243.

Ding D, Ren Y C, Li S Q et al. 1995. Study on storm deposits in the Yellow River delta and adjacent area. *Marine Geology and Quaternary Geology*, **15**(3): 25-34. (in Chinese with English abstract)

Dondurur D, Çifçi G, Drahor M G et al. 2011. Acoustic evidence of shallow gas accumulations and active pockmarks in the İzmir Gulf, Aegean sea. *Marine and Petroleum Geology*, **28**(8): 1 505-1 516.

Dunn S L, Vun P L, Chan A H C et al. 2006. Numerical modeling of wave-induced liquefaction around pipelines. *Journal of Waterway*, *Port*, *Coastal*, *and Ocean Engineering*, **132**(4): 276-288.

Feng X L, Lin L, Zhuang Z Y et al. 1999. The relationship between geotechnical parameters and sedimentary environment of soil layers since holocene in modern Huanghe subaqueous delta. *Coastal Engineering*, **18**(4): 1-7. (in Chinese with English abstract)

Hammer Ø, Webb K E, Depreiter D. 2009. Numerical simulation of upwelling currents in pockmarks, and data from the Inner Oslofjord, Norway. *Geo-Marine Letters*, **29**(4): 269-275.

Harrington P K. 1985. Formation of pockmarks by pore-water escape. *Geo-Marine Letters*, **5**(3): 193-197.

Hovland M, Judd A G. 1988. Seabed Pockmarks and Seepages. Graham and Trotman, London. 293p.

Jeng D S. 2003. Wave-induced sea floor dynamics. *Applied Mechanics Reviews*, **56**(4): 407-429.

Jia Y G, Dong H G, Shan H X et al. 2007. Study of characters and formation mechanism of hard crust on tidal flat of Yellow River estuary. *Rock and Soil Mechanics*, **28**(10): 2 029-2 035. (in Chinese with English abstract)

Judd A G, Hovland M. 2007. Seabed Fluid Flow: the Impact on Geology, Biology, and the Marine Environment. Cambridge University Press, UK. 475p.

Kilhams B, McArthur A, Huuse M et al. 2011. Enigmatic large-scale furrows of Miocene to Pliocene age from the central North Sea: current-scoured pockmarks? *Geo-Marine Letters*, **31**(5-6): 437-449.

King L H, MacLean B. 1970. Pockmarks on the Scotian shelf. *Geological Society of America Bulletin*, **81**(10): 3 141-3 148.

Li H D, Yang Z S, Wang H J et al. 2006. Factors of geohazards in the modern Yellow River delta. *Marine Geology and Quaternary Geology*, **26**(4): 37-43. (in Chinese with English abstract)

Liu H J, Fang Z M, Zhang M S. 2012. Analysis of seepage of unsaturated silty seabed under cycle loads. *Periodical of Ocean University of China*, **42**(12): 115-119. (in Chinese with English abstract)

Liu H J, Wang H, Zhang M S et al. 2013a. Analysis of wave-induced dynamic response of silty seabed in Yellow River delta. *Rock and Soil Mechanics*, **34**(7): 2 065-2 071. (in Chinese with English abstract)

Liu H J, Zhang M S, Jia Y G et al. 2006. Analysis of seabed stability under wave loading. *Rock and Soil Mechanics*, **27**(6): 986-990. (in Chinese with English abstract)

Liu X L, Jia Y G, Zheng J W et al. 2013b. Experimental evidence of wave-induced inhomogeneity in the strength of silty seabed sediments: Yellow River Delta, China. *Ocean Engineering*, **59**: 120-128.

Mory M, Michallet H, Bonjean D et al. 2007. A field study of momentary liquefaction caused by waves around a coastal structure. *Journal of Waterway*, *Port*, *Coastal*, *and Ocean Engineering*, **133**(1): 28-38.

Moss J L, Cartwright J, Cartwright A et al. 2012. The spatial pattern and drainage cell characteristics of a pockmark field, Nile Deep Sea Fan. *Marine and Petroleum Geology*, **35**(1): 321-336.

Pau M, Gisler G, Hammer Ø. 2014. Experimental investigation of the hydrodynamics in pockmarks using particle tracking velocimetry. *Geo-Marine Letters*, **34**(1): 11-19.

Prior D B, Yang Z S, Bornhold B D et al. 1986. Active slope failure, sediment collapse, and silt flows on the modern subaqueous Huanghe (Yellow River) delta. *Geo-Marine Letters*, **6**(2): 85-95.

Sakai T, Hatanaka K, Mase H. 1992. Wave-induced effective stress in seabed and its momentary liquefaction. *Journal of Waterway*, *Port*, *Coastal*, *and Ocean Engineering*, **118**(2): 202-206.

Salmi M S, Johnson H P, Leifer I et al. 2011. Behavior of methane seep bubbles over a pockmark on the Cascadia continental margin. *Geosphere*, **7**(6): 1 273-1 283.

Santos I R, Eyre B D, Huettel M. 2012. The driving forces of porewater and groundwater flow in permeable coastal sediments: a review. *Estuarine*, *Coastal and Shelf Science*, **98**: 1-15.

Sassa S, Sekiguchi H. 1999. Wave-induced liquefaction of beds of sand in a centrifuge. *Géotechnique*, **49**(5): 621-638.

Sultan N, Marsset B, Ker S et al. 2010. Hydrate dissolution as a potential mechanism for pockmark formation in the Niger delta. *Journal of Geophysical Research*: *Solid Earth*, **115**(B8): 1-33.

Sumer B M, Fredsøe J. 2002. The Mechanics of Scour in the Marine Environment. World Scientific, Singapore.

Tzang S Y, Ou S H. 2006. Laboratory flume studies on monochromatic wave-fine sandy bed interactions: part 1. Soil fluidization. *Coastal Engineering*, **53**(11): 965-982.

Xu D S, Wang R, Meng Q S et al. 2010. Experimental research on in-situ mechianical properties of silt in Yellow River delta. *Chinese Journal of Rock Mechanics and Engineering*, **29**(2): 409-416. (in Chinese with English abstract)

Xu G H, Sun Y F, Wang X et al. 2009. Wave-induced shallow slides and their features on the subaqueous Yellow River delta. *Canadian Geotechnical Journal*, **46**(12): 1 406-1 417.

Yamamoto T, Koning H L, Sellmeijer H et al. 1978. On the response of a poro-elastic bed to water waves. *Journal of Fluid Mechanics*, **87**(1): 193-206.

Yang S L, Shen W Q, Yang Z S. 1995. The mechanism analysis of seafloor silt liquefaction under wave loads. *Chinese Journal of Geotechnical Engineering*, **17**(4): 28-37. (in Chinese with English abstract)

Zen K, Yamazaki H. 1990. Mechanism of wave-induced liquefaction and densification in seabed. *Soils and Foundations*, **30**(4): 90-104.